# Sequential Unfolding of Individual Helices of Bacterioopsin Observed in Molecular Dynamics Simulations of Extraction from the Purple Membrane

Michele Seeber,* Francesca Fanelli,† Emanuele Paci,*‡ and Amedeo Caflisch*
*Department of Biochemistry, University of Zurich, Zurich, Switzerland; †Dulbecco Telethon Institute, Department of Chemistry, University of Modena and Reggio Emilia, Italy; and ‡Physics and Astronomy, University of Leeds, Leeds, United Kingdom

ABSTRACT Multiple molecular dynamics simulations of bacterioopsin pulling from its C-terminus show that its $\alpha$-helices unfold individually. In the first metastable state observed in the simulations, helix G is unfolded at its C-terminal segment while the rest of helix G (residues 200–216) is folded and opposes resistance because of a salt-bridge network consisting of Asp-212 and Lys-216 on helix G and Arg-82 and Asp-85 on helix C. Helix G unfolds inside the bundle because the external force is applied to its C-terminal end in a direction perpendicular to the surface of the membrane. Inversely, helix F has to flip by 180° to exit from the membrane because the applied force and the helical N-C axis point in opposite directions. At the highest peak of the force, which cannot be interpreted in single-molecule force spectroscopy experiments, helix F has a pronounced kink at Pro-186. Mutation of Pro-186 and/or the charged side chains mentioned above, which are involved in very favorable electrostatic interactions in the low-dielectric region of the membrane, are expected to reduce the highest peak of the force. Helices E and D unfold in a similar way to helices G and F, respectively. Hence, the force-distance profile and sequence of events during forced unfolding of bacterioopsin are influenced by the up-and-down topology of the seven-helix bundle. The sequential extraction of individual helices from the membrane suggests that the spontaneous (un)folding of bacterioopsin proceeds through metastable bundles of fewer than seven helices. The metastable states observed in the simulations provide atomic level evidence that corroborates the interpretation of very recent force spectroscopy experiments of bacteriorhodopsin refolding.

## INTRODUCTION

Integral membrane proteins are involved in a wide variety of functions like photosynthesis, transport of ions and small molecules, and signal transduction. They either consist of a varying number of $\alpha$-helices (e.g., G-protein coupled receptors (1), aquaporin (2), and the ammonia channel (3)) or they adopt a $\beta$-barrel fold containing between 8 and 22 $\beta$-strands (4). The former are much more common than the latter, which are exclusively found in the outer membrane of Gram-negative bacteria. However, despite the relative abundance of membrane proteins among all proteins and despite the fact that they represent the majority of the targets for existing drugs (5,6), only a few structures have been solved so far. Moreover, the mechanism of folding and assembly within the membrane is not clear (7).

Bacteriorhodopsin (BR) is one of the most extensively studied integral membrane proteins (8–10). BR is a light-driven proton pump and its photoactive retinal, which is bound covalently through the Schiff base to Lys-216, is embedded in seven closely packed transmembrane $\alpha$-helices (termed A–G) arranged in an up-and-down topology (Fig. 1, *top*). In the purple membrane BR adopts a trimeric state stabilized by the presence of lipids in the central compartment, which has a nearly cylindrical shape (11). High-resolution atomic force microscopy (AFM) topography of the cytoplasmic surface of a wild-type purple membrane shows that trimeric BR molecules arrange in a hexagonal lattice (12).

The forced unfolding and extraction from the purple membrane of BR and of its retinal-free form, bacterioopsin (BO), have been investigated in depth by combining AFM imaging with single-molecule force spectroscopy (12–15). AFM is a powerful method to shed light on mechanical protein unfolding or unbinding of a protein-ligand complex at the single molecule level, removing the averaging over large ensembles of molecules implied in other biophysical/biochemical approaches. Two different AFM techniques are available to probe the mechanical resistance of biomolecules. In the force-ramp method, a time-dependent force is applied (16), while in the so-called force-clamp method, the force is held constant (17). Based on the force-ramp method, dynamic force spectroscopy (18) has provided a deep insight into the unbinding mechanism of a variety of biological complexes, such as the (strept)avidin-biotin complex (19) and the complex between L-selectin and various binding partners (20).

However, it is desirable to relate the information on unfolding or unbinding provided by the AFM techniques to the changes in tertiary and secondary structure. For this purpose, AFM observations can be complemented with molecular dynamics (MD) simulations, which describe the behavior of individual molecules at an atomic level of detail. Constant-velocity MD (termed also steered-MD and abbreviated as SMD) and constant force MD (CFMD) simulations mimic the force-ramp and the force-clamp method of AFM, respectively, and have been widely used to study protein-ligand unbinding (21–25) and protein unfolding (26–29). Very different

*Submitted May 9, 2006, and accepted for publication July 14, 2006.*

Address reprint requests to E. Paci, E-mail: e.paci@leeds.ac.uk; or to A. Caflisch, E-mail: caflisch@bioc.unizh.ch.



0006-3495/06/11/3276/09 $2.00

doi: 10.1529/biophysj.106.088591

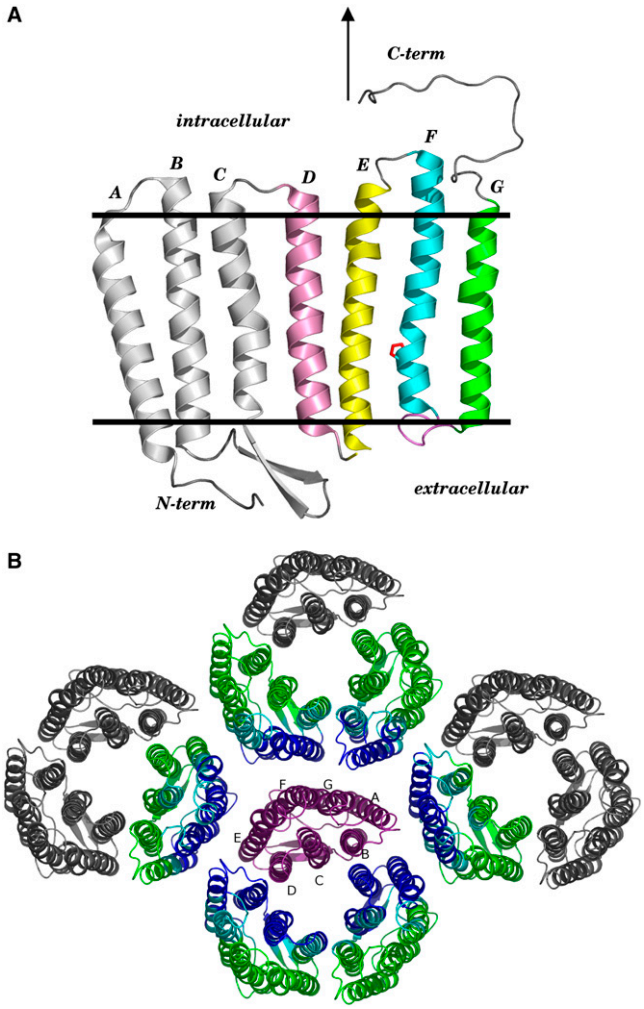


FIGURE 1 BO topology and heptamer within the tetra-trimeric assembly. (*Top*) Schematic model of the seven $\alpha$-helices of BO and their orientation in the membrane. The picture was obtained by ''manually opening'' the three-dimensional arrangement of the seven-helix bundle into a plane. The side chain of Pro-186 is shown in red. The direction of pulling is indicated by an arrow. (*Bottom*) Top view on the BO tetra-trimer from the intracellular side. The pulling force acts on the C-terminus of the central BO molecule, which is colored in magenta. The heptamer considered in the simulations is in color whereas the five most external BO molecules, which were neglected in the simulations, are in gray. The residues in the six BO molecules surrounding the ''pulled'' BO are colored according to the constraints used in the simulations (i.e., fully flexible, *blue*; harmonically restrained, *cyan*; and fixed, *green*).

timescales are involved in AFM experiments and SMD/CFMD simulations because force spectroscopy experiments are typically carried out on the millisecond timescale or slower while simulations are currently limited to nanoseconds. Nevertheless, simulations have helped to interpret consistently experimental observations and have been even used to formulate predictions subsequently verified by in vitro experiments (18,27,30–36).

By using a combination of AFM imaging and single-molecule force spectroscopy Gaub, Müller, and their coworkers have characterized the mechanical resistance and sequence of unfolding events during forced extraction of single BR and BO molecules from native purple membrane patches (12–15). They have monitored the mechanical stability of individual structural elements of the photoreceptor during pulling from the C-terminus (i.e., from the cytoplasmic side) and have investigated the influence of different pH values (from 4.2 to 10) (15), temperature values (from 8 to 52°C) (13), pulling velocities (from 10 nm $s^{-1}$ to 5.23 $\mu$m $s^{-1}$) (14), and oligomerization state (from monomeric to trimeric) (37). Similar force-distance profiles were recorded for BR and BO (15). Two mechanisms of forced unfolding have been proposed on the basis of the single-molecule experiments. One mechanism postulates the pairwise extraction of helices (i.e., G and F; E and D; and C and B, see Fig. 1), while the other postulates the sequential unfolding of individual helices (i.e., G, F, E, D, C, and B, in this order). Interestingly, pathways with pairwise unfolding of transmembrane $\alpha$-helices were shown to have higher probability at low pulling speed, high temperature or in the monomeric state, whereas at high pulling speed, low temperature, or in the trimeric state, individual $\alpha$-helix unfolding was more probable—i.e., each $\alpha$-helix was kinetically stable and its extraction constituted a barrier against mechanical unfolding (13,14,37). Furthermore, intermediate states in the mechanical unfolding of BR have been suggested to originate from kinks in helices F and B by a recent force-modulation spectroscopy analysis (38). It is important to note that the unfolding barriers observed by pulling from the cytoplasmic side are consistent with those recorded recently by pulling from the N-terminal extracellular side (39), as well as with the controlled single-molecule refolding monitored by gradually lowering the AFM tip to allow BR to refold into the membrane (40).

In this article, the unfolding of BO is investigated by multiple implicit solvent SMD and CFMD simulations of forced extraction from the purple membrane. Given the very similar force-distance profiles obtained in vitro for BR and BO (15) it was decided to perform all simulations with only one of the two forms of the photoreceptor. BO was preferred to BR because it is not clear how to obtain retinal parameters consistent with the implicit membrane/water model. The present study is motivated by the lack of a unique, clearcut interpretation of the force-extension profiles recorded in single-molecule experiments of photoreceptor unfolding (14,39). In particular, for the early steps of extraction, nonspecific interactions between the purple membrane surface and the AFM tip do not allow a detailed analysis of the first force peak (which is the highest one), and has been suggested to correspond to the unfolding and extraction of helices G and F (12,13,15). A simulation system has been ad-hoc developed to effectively mimic the extraction process in a native-like environment. A heptameric system has been assembled from BO trimers by exploiting the hexagonal lattice symmetry of BO in the native purple membrane (12). Pulling

by SMD and CFMD is applied to the BO molecule located at the center of the hexagonal arrangement (Fig. 1, *bottom*). The atoms in the BO molecules are simulated explicitly, while the lipids in the membrane as well as the aqueous environment surrounding the membrane are accounted for by an implicit model (41). The use of a mean-field approximation for the lipids is justified by the fact that they mainly interact with helices B, C, and D in the central compartment of the trimer (11), whereas the present simulation study focuses on the extraction of helices E, F, and G, which are involved in intra- and intertrimer contacts (Fig. 1, *bottom*). Moreover, because of the mainly hydrophobic environment, water molecules are not likely to penetrate into the membrane and replace intrahelical hydrogen bonds during the early phase of unfolding, which justifies the use of an implicit treatment of the solvent. The polypeptide chains surrounding the central (i.e., pulled) BO molecule are restrained to approximate the tight packing of BO molecules and preserve as much as possible the native environment of the purple membrane. The computational experiments are aimed at gaining insight, at an atomic level of detail, into the inter- and intramolecular interactions stabilizing the ''pulled'' BO molecule. The simulation results suggest that the initial metastable states are a consequence of some key residues, while the unfolding pathways and force-distance profile reflect the transmembrane up-and-down topology of the seven-helix bundle.

## MODEL AND METHODS

### Modeling of BO oligomers

As mentioned in the Introduction, BR adopts a trimeric state in the purple membrane (11). The trimers partition the lipid bilayer into two discontinuous compartments: a central one cylindrically enclosed by the BR trimer with space for six lipids (11) and an outer phase with lipids of unknown chemical nature (42). High-resolution AFM topography of the cytoplasmic surface of a wild-type purple membrane clearly shows that BR assembles in trimers arranged in a hexagonal lattice (12). To approximate the tight packing in the native purple membrane a polymeric bundle of retinal-free BR (i.e., BO) molecules has been modeled in which a central monomer is completely surrounded by other BO monomers. The high resolution structure of trimeric BR (PDB http://www.rcsb.org/pdb/ code: 1BRR (11)) and the AFM topography (12) were used to build an assembly of four BO trimers, namely the BO tetra-trimer (Fig. 1, *bottom*). The monomer C in the ABC trimer, which is better resolved than the other two because it lacks only residues 1 and 232–247, was completed at the N- and C-termini using MODELLER (43) and employed in place of the other two monomers in the trimer. The homogeneous trimer resulting from this replacement was then employed as a building block to achieve a tetra-trimeric assembly. The assembly of two trimers was done manually, according to the relative positions seen in the AFM topography. Once obtained the di-trimer, the tetra-trimer assembly was generated by applying the hexagonal symmetry. Two different tetra-trimeric models were built for the present simulation study. They differ slightly in the interatomic distances at the inter-trimer interface, which consists mainly of helix A-helix A and helix E-helix F contacts. One of the two models has a tighter trimer-trimer packing than the other. Since the information gained from AFM imaging of purple membrane is qualitative, no set of distances could be defined as standard. Therefore, two different models were employed to explore the dependency of the results on the details of the supramolecular assembly.

Computational experiments were then carried out on heptameric BO. Three heptameric BO assemblies were derived from the two tetra-trimeric models described above by deleting the five monomers not in contact with the central monomer (see Fig. 1, *bottom*). The first BO heptamer was derived from the tetra-trimer model with looser interface and consists of full-length (247 residues) identical BO monomers. Another BO heptamer was generated by C-terminal truncation of residues 234–247. The third BO heptamer was derived from the tetra-trimer model with tighter interface and consists of 232-residue monomers truncated at the C-terminus. All monomers in a tetra-trimer have the same sequence length. The truncated forms were built to evaluate to which extent the results of pulling simulations depend on the length and conformation of the C-terminal segment whose structure is ill-defined. The retinal-free BO structure was obtained by removing the retinal before the minimization and equilibration procedure described in the next subsection.

### Molecular dynamics

Minimizations and molecular dynamics simulations were performed using the CHARMM program (44). A united-atom model (param19 (45)) was used with an implicit membrane/water model IMM1 (41)). The latter is an extension of the EEF1 (46) implicit water model to heterogeneous membrane-aqueous media. The dielectric screening parameter ($a$ in Eq. 10 of (41)) and the nonpolar core thickness were set equal to 0.70 and 32 Å, respectively. Minimizations were carried out by using 200 steps of steepest descent followed by 500 steps of conjugate gradient minimization. MD simulations were carried out on the minimized coordinates. The lengths of the bonds involving the hydrogen atoms were restrained according to the SHAKE algorithm, allowing an integration time step of 2 fs. The systems were heated to 300 K with 3 K rise every 5000 steps during 500,000 steps. After heating, the systems were allowed to equilibrate for 200 ps.

Two types of restraints were applied to different parts of the macromolecular assembly to preserve the polymeric structure and reduce the purple membrane from an infinite two-dimensional crystal to a finite-size system. Given the almost paracrystalline organization of BR monomers in the purple membrane, restraints are instrumental in avoiding displacement of the proteins that constitute the environment of the pulled protein. Indeed, the AFM experiments show that BR monomers do not reorganize to fill the cavity originating from the single-molecule extraction (12). Atoms lying more than 18 Å from any atom of the central (pulled) BO were kept fixed, thus creating a ''rigid'' shell, in agreement with AFM topography showing stable holes in purple membrane upon BO pulling (12). Atom lying at a distance between 13 Å and 18 Å were harmonically restrained to create a buffer zone. Finally, the remaining atoms, i.e., those of the central monomer and those close to it ($<$13 Å apart), were not subjected to any restraint (Fig. 1, *bottom*). Alternative setups were tried before choosing the implicit solvent/protein cage model. BO monomers in an implicit membrane/water system showed artifacts such as anomalous rotation of the protein during pulling, violating experimental observation.

Pulling simulations were carried out by means of the AFM module (28) implemented in CHARMM. Three different pulling methods can be employed through the AFM module. One is the constant-force MD (CFMD) method, which simply applies a constant force to two selected atoms. The other method is steered-molecular dynamics (SMD), in which the force applied between two selected atoms is proportional to the difference between the distance of the two atoms and a linearly increasing length. The third method is biased-molecular dynamics (BMD), in which the force applied to the two atoms is proportional to the difference between the interatomic distance and the maximum distance previously reached. SMD and CFMD were used in this work. The former method was aimed at reproducing the force patterns achieved by in vitro experiments. The latter was instrumental in inferring hypotheses on the unfolding process at the atomic detail. In all simulations the force was applied to the $C_\alpha$ atom of the C-terminal residue

and a dummy atom positioned far away from the membrane, i.e., at a distance of 30 nm on the extracellular side. In this way the force on the BO molecule is effectively directed perpendicularly to the membrane plane.

Table 1 lists length and type of simulations. Eighteen SMD runs were performed using a force constant of 100 pN/nm, which corresponds to that of the AFM cantilever. On the other hand, the speed is more than six-orders-of-magnitude higher, i.e., 0.1 nm/ps to cover a distance of 70 nm in 0.7 ns. Three SMD simulations at a speed of 0.05 nm/ps and force constant of 250 pN/nm were performed to evaluate the influence of the pulling speed. In the CFMD runs, the values of the force ranged from 350 pN to 600 pN and the simulation length was 8 ns. The aggregate simulation time was 23 ns and 96 ns for the SMD and CFMD runs, respectively. Furthermore, three control simulations of 10 ns each were performed to check the stability of the heptameric model and eventual deviations from the x-ray structure.

## RESULTS AND DISCUSSION

### Control simulations

Before studying the forced extraction of BO from the membrane, three control runs of 10 ns each were performed without any external force but using the same heptameric assembly and simulation protocol as in the pulling simulations. In the three control runs, BO is stable in its native transmembrane arrangement. Fig. 2 shows that in one of the three control runs the $C_\alpha$ root mean-square deviation (RMSD) from the x-ray structure reaches a plateau value of ~2.3 Å after 3 ns. Both the helical structure and interhelical segments are preserved with individual helix $C_\alpha$ RMSD values ranging between 0.7 Å and 1.7 Å. Similar deviations were observed for the other two control runs.

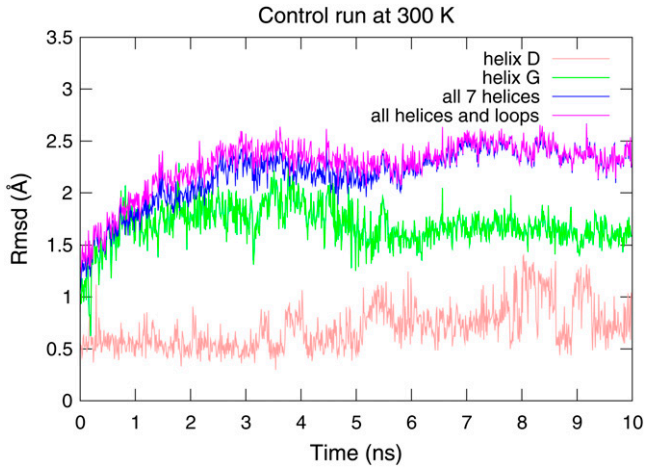


FIGURE 2 Structural stability during MD without external forces. $C_\alpha$ RMSD from the x-ray structure along a 10-ns control run of BO at 300 K. The $C_\alpha$ RMSD of residues 9–225 is calculated for the BO molecule in the center of the heptamer, i.e., the BO molecule in magenta in the bottom of Fig. 1. The same setup and restraints on the six surrounding BO molecules were used as in the pulling simulations, but no external force was applied in the control runs. The time series of the $C_\alpha$ RMSD of BO with and without interhelical segments are shown in magenta and blue, respectively. Note that the two curves almost overlap because of the very short length of the interhelical segments and the stability of the $\beta$-hairpin segment between helices B and C. The pink and green curves display the behavior of the most and least stable helix, respectively.

### Steered-molecular dynamics (SMD) simulations: force peaks

The force-distance plots extracted from the SMD simulations (Fig. 3) are in qualitative agreement with the force spectroscopy data (12,15). The results are consistent in the number of force peaks, the interpeak distances, and the relative height of the peaks. The height of the peaks decreases during the extraction because missing helices destabilize the packing, thereby reducing the anchoring interactions of the remaining helices. According to the phenomenological Bell law (47), the logarithm of the unfolding rate (or, equivalently, of the pulling speed in SMD simulations and AFM experiments) depends linearly on the applied pulling force. Thus, here as in previous simulations of forced unfolding or unbinding (33,48–50), the height of the force peaks cannot be directly compared with the experiments, due to the several orders-of-magnitude difference in pulling speed, and also the negligible viscosity of the implicit lipids and water solvent (see Model and Methods). What is not obvious is that by pulling at a high speed the explored unfolding pathways are the same, since the Bell law assumes that the unfolding force is determined by a single barrier in a unidimensional energy landscape—an oversimplification of the real multidimensional landscape where unfolding can occur through different barriers at different pulling speeds. The qualitative

**TABLE 1 Simulations performed**

| | Number of runs | Length [ns] | Velocity [nm/ps] | Force constant or force | Full unfolding |
|---|---|---|---|---|---|
| Control | 3 | 10 | — | — | 0 of 3 |
| SMD* | 18 | 1 | 0.1 | 100 pN/nm | 18 of 18 |
| | 3 | 1.6 | 0.05 | 250 pN/nm | 3 of 3 |
| CFMD† | 2 | 8 | — | 350 pN | 0 of 2 |
| | 2 | 8 | — | 400 pN | 0 of 2 |
| | 2 | 8 | — | 450 pN | 0 of 2 |
| | 5 | 8 | — | 500 pN | 5 of 5 |
| | 1 | 8 | — | 600 pN | 1 of 1 |

*An equal number of SMD runs were performed starting from each of the three heptameric models, i.e., six runs with a pulling velocity of 0.1 nm/ps and one run with 0.05 nm/ps.

†All CFMD runs were performed with the heptameric model consisting of 247-residue BO monomers.

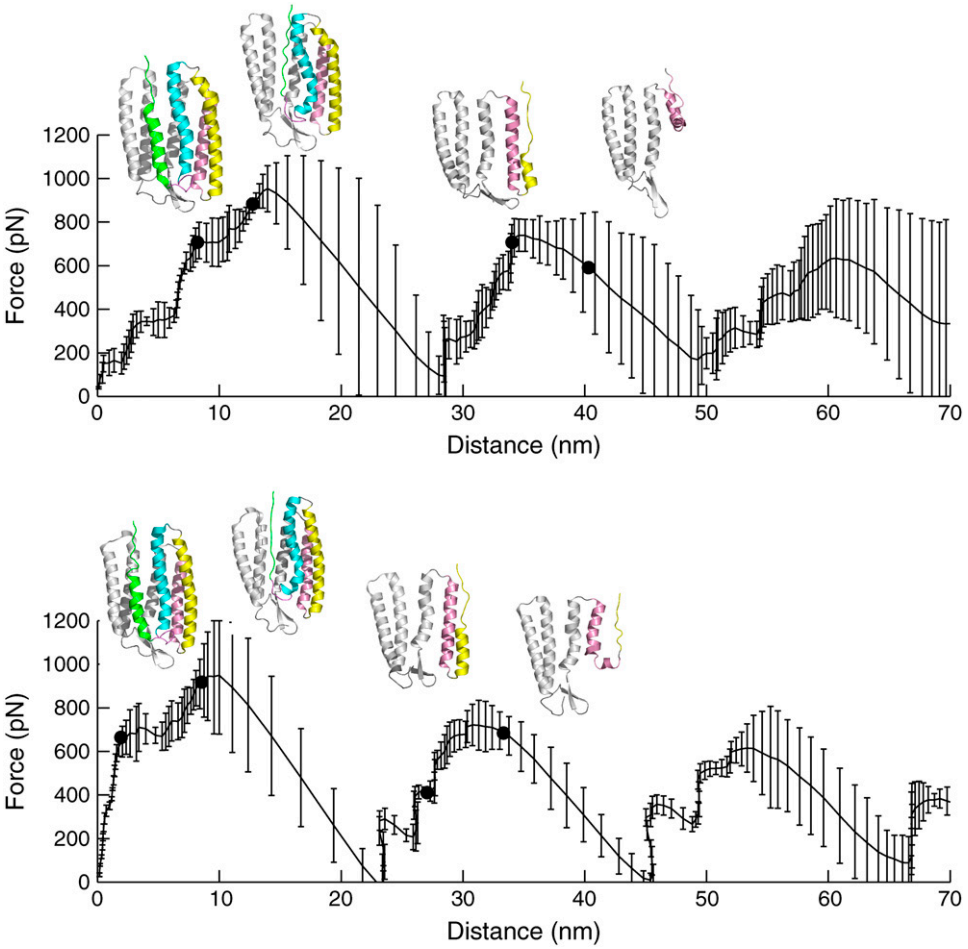


FIGURE 3 Force-distance profiles during SMD. Force-distance curves of BO in SMD simulations with pulling speed of 0.1 nm/ps and force constant of 100 pN/nm. The solid line is an average over three runs and the error bars represent standard deviations. (*Top*) Heptamer model consisting of 247-residue BO monomers. (*Bottom*) Heptamer model with tighter intertrimeric interface consisting of 232-residue BO monomers. This profile is shifted toward left by ~5 nm with respect to that of the 247-residue BO system because of the difference in the chain length. Snapshots show representative conformations along the unfolding pathway with helices colored as in the top part of Fig. 1 (i.e., *A–C*, *gray*; *D*, *pink*; *E*, *yellow*; *F*, *cyan*; and *G*, *green*). The black circles indicate the exact position along the force-distance profiles of the snapshots shown in the insets. Snapshots related to the third main peak are not shown because the final stages of the extraction are heterogeneous.

agreement with the experiment, in what concerns the number and position of the peaks, provides strong evidence that, in the specific case of BO, the unfolding mechanism is the same in a broad range of pulling speeds including those used in the experiment and in the present MD simulations.

Three main peaks are observed within the first 60 nm (Fig. 3). Both the regular spacing between the three main peaks and the relative heights (i.e., local maxima of the force) are consistent with the up-and-down topology of the seven-helix bundle and the direction of pulling. During extraction from the membrane (i.e., mechanical unfolding from the C-terminus) helices G, E, and C are pulled in a direction that allows them to unfold by helical stretching (Fig. 1, *top* and Fig. 3). On the contrary, helices F, D, and B cannot stretch during pulling because the pulling direction is opposite to the helical stretch direction; in other words, helices F, D, and B have to flip by 180° before leaving the membrane. The time series of the secondary structure content during the SMD runs show that extraction of helices G and E involves metastable states with partial helical conformation (Fig. 4). Furthermore, the stretching of helix E results in the formation of a short $3_{10}$-helical segment. The shoulder preceding the highest peak originates from the partial unfolding of helix G whose N-terminal segment (residues 200–216) is still helical at pulling distances below 10 nm. The highest peak of ~1000 pN in Fig. 3 corresponds to the high mechanical resistance encountered by helix F whose unfolding is preceded by a kinking hindered by the rest of the protein. The second main peak originates from the partial unfolding of helix E at a distance of ~37 nm and 32 nm for the 247-residue and 232-residue model of BO, respectively. The unfolding of helix E is analogous to that of helix G (Fig. 4). In fact, the height of the second main peak (~800 pN) is similar to the shoulder preceding the first main peak (Fig. 3). Helix D has to flip to be pulled out of the membrane, but structural destabilization due to absence of helices G, F, and E allows this to happen without another force peak. The third main peak is much less defined than the first two, and is mainly due to the resistance opposed by the remaining helices C, B, and A to complete removal from the membrane. Interestingly, the force-distance profiles (Fig. 3) and main sequence of events (Fig. 4 and next subsection) are essentially identical for the three structural models probed in this study. This similarity indicates that the simulation results do not depend on the fine details of the structural models, thus supporting the robustness of the computational protocol and the choice of restraints.

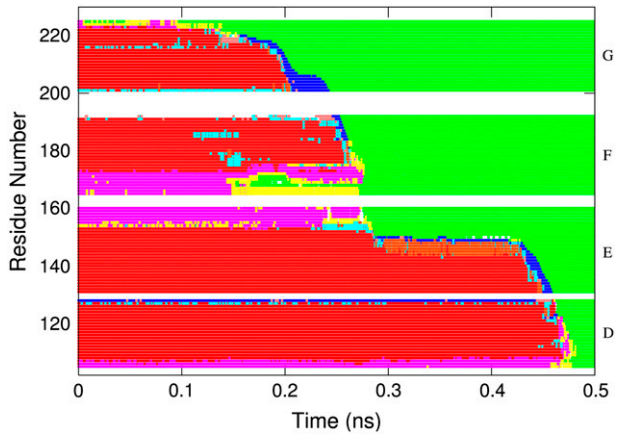


FIGURE 4 Helical unfolding during SMD. Time series of secondary structure loss along the first 0.5 ns of SMD pulling using the heptameric model consisting of 247-residue BO monomers. Helix G (residues 200–225) unfolds gradually and then exits the membrane/protein environment, while helix F (residues 164–191) is extracted and unfolds almost all at once after having rotated end-to-end. The unfolding of the C-terminal part of helix E is almost concomitant with the extraction of helix F, while the N-terminal half of helix E is metastable and generates the second main peak of the force. Helix D behaves like helix F. Helices A–C are not shown because their structure is stable during the first 0.5 ns. (Color code: *red*, $\alpha$-helices embedded in the membrane; *magenta*, $\alpha$-helices at the membrane/solvent interface; *cyan*, $\alpha$-helical turn inside the membrane; *yellow*, $\alpha$-helical turn outside the membrane; *blue*, loop inside the membrane; *green*, loop outside the membrane; *orange*, $3_{10}$ helix inside the membrane; and *pink*, bend inside the membrane.)

## Constant force molecular dynamics (CFMD) simulations: sequence of events and metastable states

The two pulling techniques used in the present simulation study yield consistent results but also complementary information. The main advantage of SMD is the possibility of defining a timescale for the process to be investigated. Furthermore, SMD (but not CFMD) yields force-distance profiles that can be directly compared with the force spectroscopy data. On the other hand, CFMD is better suited to identify long-lived metastable states. CFMD requires running several simulations at different values of the applied force because low forces usually do not achieve full unfolding while high forces do not allow us to isolate intermediates. The analysis of the simulations focuses on the four C-terminal helices D–G for two reasons. First, despite the eightfold longer simulation time of the CFMD runs with respect to the SMD runs, the former reach only partial extraction at low values of the applied force. Second, the molecular system is not completely free to rearrange upon extraction of the C-terminal helices because of the rigidity of the external shell of residues in the heptameric model (*green regions* in Fig. 1, *bottom*). Hence, it is likely that the extraction of the N-terminal helices is slightly facilitated by the reduced packing of the solute, which is not the case for the C-terminal helices.

As mentioned above, the sequence of events observed with SMD (Figs. 3 and 4) and CFMD (Fig. 5) are essentially identical and provide further evidence for the interpretation of the force-distance profiles obtained by single-molecule force spectroscopy at high pulling speed (14). The events in the forced unfolding runs can be enumerated as follows:

1. Starting from its C-terminal end, helix G unravels progressively within the membrane; the N-terminal segment of helix G is kinetically stable in CFMD runs at low force (350–450 pN, Fig. 5). The stability is due, at least in part, to a network of salt bridges involving Asp-212 and Lys-216 on helix G and Arg-82 and Asp-85 on helix C (Fig. 6). These electrostatic interactions are particularly

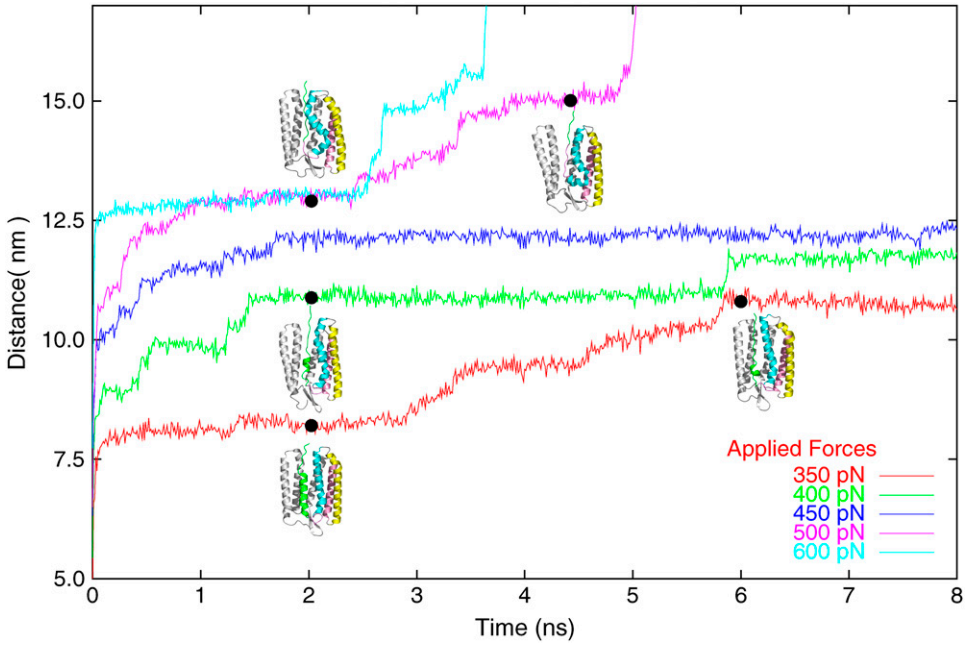


FIGURE 5 Metastable states observed by CFMD. Time series of the displacement of the pulled atom from its initial position in CFMD runs at different forces (350–600 pN) using the heptameric model consisting of 247-residue BO monomers. The insets show snapshots extracted from the plateau-regions with helices colored as in the top part of Fig. 1 (i.e., *A–C*, *gray*; *D*, *pink*; *E*, *yellow*; *F*, *cyan*; and *G*, *green*). The black circles indicate the positions of the snapshots along the trajectories.

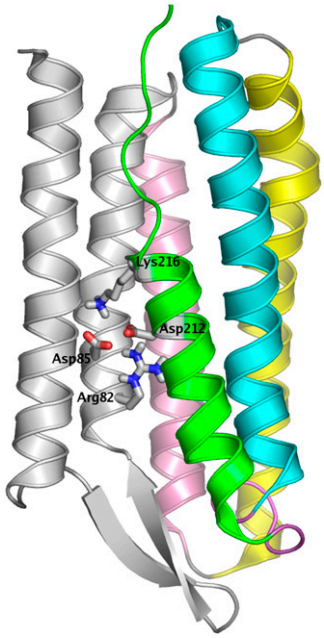


FIGURE 6 Network of salt bridges stabilizing the first mechanical unfolding intermediate. Representative snapshot at 8 nm displacement during one of the SMD runs. The side chains of Asp-212 and Lys-216 on helix G are involved in a salt-bridge network with Arg-82 and Asp-85 on helix C. Helices B–G are colored as in the top part of Fig. 1 (while, for visual clarity, helix A is not shown).

stable because of the low dielectric environment in the interior of the seven-helix bundle in a region corresponding to the middle of the bilayer.

2. Upon complete unfolding of helix G the loop FG enters into the remaining six-helix bundle. A pronounced kink of helix F at Pro-186 corresponds to the most populated kinetic intermediate in the SMD runs and in most CFMD runs. This intermediate is located at a distance of 12.5 nm for the 247-residue model (see *insets* of Fig. 5) and corresponds to the main force peak in SMD (Fig. 3, *top*). Notably, a similar intermediate with a kink at Pro-186 has been postulated on the basis of recent force modulation spectroscopy data (38).
3. In contrast to helix G, helix F unfolds in a single step which is concomitant to its end-to-end flipping.
4. The loop EF yields to the pulling force without resistance because it is located on the cytosolic side (Fig. 1, *top*); helix E unfolds in a way similar to helix G because its N-C axis points in the same direction as the pulling force. In fact, the second peak in the force-distance plot originates from a metastable state occurring upon unfolding of ~12 of the 30 residues of helix E. This metastable state is due to intermonomer hydrogen bonds involving the side chains of Tyr-147 and Tyr-150, which interact with residues of helices A and B from a monomer within the same trimeric subunit, and with residues of helix F from another trimer. Taken together, the SMD and CFMD simulation results provide a consistent picture of the influence of the seven-helix up-and-down topology in forced unfolding and, at the same time, highlight the stabilizing role of a few charged and aromatic side chains.

## CONCLUSIONS

Despite the large difference in timescales (1–10 ns in MD simulations versus $10^{-2}$–10 s in single-molecule force spectroscopy), the MD simulations of forced unfolding of BO from the purple membrane are useful to complement the single-molecule force spectroscopy data and help the interpretation of the force peaks. In particular, the AFM analysis does not provide detailed information on the initial phase of forced unfolding (i.e., the extraction of helices G and F) whereas the simulation results are most informative on this very initial phase.

Four main points emerge from the present simulation study and comparison with single-molecule force spectroscopy analysis. First, the sequential unfolding of individual helices observed in the simulations is consistent with the statistical predominance of individual versus pairwise helical unfolding in force-distance profiles recorded at high pulling speed (14), low temperature (13), and for the trimeric assembly (37). No pairwise helical unfolding event was observed in the simulations. Second, the MD results are useful to interpret the highest force peak, which originates from the resistance encountered during the end-to-end flipping of helix F in the bundle consisting of helices A–E. This simulation result is novel while the metastable state with pronounced kinking at Pro-186 provides strong evidence to a recent interpretation of the force-distance profiles of BR (38). Third, despite the importance of the side-chain interaction patterns that determine some of the initial intermediate states (e.g., the salt-bridge network consisting of Asp-212 and Lys-216 on helix G and Arg-82 and Asp-85 on helix C) the force-distance profile is mainly a consequence of the transmembrane topology and pulling direction. The importance of topology is consistent with the remarkable similarity in the force-distance curves of BR and halorhodopsin (a light-driven chloride pump from *Halobacterium salinarum*) as previously observed by AFM (51). In fact, BR and halorhodopsin have only ~30% sequence identity but almost identical three-dimensional structure, indicating that different residues can contribute to indistinguishable stabilizing elements. Interestingly, some of the residues contributing to the metastable states observed in the simulations (i.e., Pro-186 as well as Arg-82, Asp-212, and Lys-216) are conserved in BR and halorhodopsin. Point mutations of these residues (e.g., Pro-186-Ala and/or Asp-212-Ala) are predicted to modulate the force-distance profile because of their destabilizing effect on the intermediate states. Finally, it is difficult to speculate on the sequence of events of transmembrane protein folding in vivo (i.e., in the absence of force) using the available experimental and simulation data on forced unfolding and extraction from the purple membrane. Yet, the sequential unfolding

of individual helices indicates that bundles of less than seven helices are structurally (i.e., kinetically) stable on timescales ranging from nanoseconds, as observed in this simulation study, to seconds, as suggested from the interpretation of force-distance plots obtained by single-molecule force spectroscopy. Notably, a number of folding intermediates of BR were recently detected by an AFM study in which refolding was promoted by gradually lowering the tip (40).

We are grateful to R. Pellarin, M. Cecchini, F. Rao, and U. Haberthür for helpful discussions and technical help. We thank A. Widmer (Novartis Pharma, Basel) for providing the molecular modeling program Wit! P, which was used for visual analysis of the trajectories. Pictures were produced with the PyMOL (52) program. The simulations were performed on the Matterhorn Beowulf cluster at the Computing Center of the University of Zurich. We thank C. Bolliger, T. Steebock, and Dr. A. Godknecht for setting up and maintaining the cluster.

This work was supported by a grant from the Swiss National Science Foundation to A.C.

## REFERENCES

1. Palczewski, K., T. Kumasaka, T. Hori, C. A. Behnke, H. Motoshima, B. A. Fox, I. L. Trong, D. C. Teller, T. Okada, R. E. Stenkamp, M. Yamamoto, and M. Miyano. 2000. Crystal structure of rhodopsin: a G-protein coupled receptor. *Science*. 289:739–745.
2. Sui, H., B. G. Han, J. K. Lee, P. Walian, and B. K. Jap. 2001. Structural basis of water-specific transport through the aqp1 water channel. *Nature*. 414:872–878.
3. Khademi, S., J. O'Connell, J. Remis, Y. Robles-Colmenares, L. J. W. Miercke, and R. M. Stroud. 2004. Mechanism of ammonia transport by Amt/MEP/Rh: structure of AmtB at 1.35 Å. *Science*. 305:1587–1594.
4. Schulz, G. 2002. The structure of bacterial outer membrane proteins. *Biochim. Biophys. Acta*. 1565:308–317.
5. Hopkins, A., and C. R. Groom. 2002. The druggable genome. *Nat. Rev. Drug Discov.* 1:727–730.
6. Sanders, C., and J. K. Myers. 2004. Disease-related misassembly of membrane protein. *Annu. Rev. Biophys. Biomol. Struct*. 33:25–51.
7. Bowie, J. U. 2005. Solving the membrane protein folding problem. *Nature*. 438:581–589.
8. Haupts, U., J. Tittor, and D. Oesterhelt. 1999. Closing in on bacteriorhodopsin: progress in understanding the molecule. *Annu. Rev. Biophys. Biomol. Struct*. 28:367–399.
9. Luecke, H., B. Schobert, H. Richter, J. Cartailler, and J. Lanyi. 1999. Structure of a bacteriorhodopsin at 1.55 Å resolution. *J. Mol. Biol*. 291: 899–911.
10. Pebay-Peyroula, E., G. Rummel, J. Rosenbuch, and E. Landau. 1997. X-ray structure of bacteriorhodopsin at 2.5 Ångstroms from microcrystals grown in lipidic cubic phases. *Science*. 277:1676–1681.
11. Essen, L.-O., R. Siegert, W. D. Lehmann, and D. Oesterhelt. 1998. Lipid patches in membrane protein oligomers: crystal structure of the bacteriorhodopsin-lipid complex. *Proc. Natl. Acad. Sci. USA*. 95: 11673–11678.
12. Oesterhelt, F., D. Oesterhelt, M. Pfeiffer, A. Engel, H. E. Gaub, and D. J. Mueller. 2000. Unfolding pathways of individual bacteriorhodopsins. *Science*. 288:143–146.
13. Janovjak, H., M. Kessler, D. Oesterhelt, H. Gaub, and D. J. Mueller. 2003. Unfolding pathways of native bacteriorhodopsin depend on temperature. *EMBO J*. 22:5220–5229.
14. Janovjak, H., J. Struckmeier, M. Hubain, A. Kedrov, M. Kessler, and D. J. Mueller. 2004. Probing the energy landscape of the membrane protein bacteriorhodopsin. *Structure*. 12:871–879.
15. Mueller, D. J., M. Kessler, F. Oesterhelt, C. Moeller, D. Oesterhelt, and H. Gaub. 2002. Stability of bacteriorhodopsin $\alpha$-helices and loops analyzed by single-molecule force spectroscopy. *Biophys. J*. 83: 3578–3588.
16. Florin, E., V. Moy, and H. Gaub. 1994. Adhesion forces between individual ligand-receptor pairs. *Science*. 264:415–417.
17. Oberhauser, A., P. Hansma, M. Carrion-Vazquez, and J. Fernandez. 2001. Stepwise unfolding of titin under force-clamp atomic force microscopy. *Proc. Natl. Acad. Sci. USA*. 98:468–472.
18. Evans, E., and K. Ritchie. 1997. Dynamic strength of molecular adhesion bonds. *Biophys. J*. 72:1541–1555.
19. Merkel, R., P. Nassoy, A. Leung, K. Ritchie, and E. Evans. 1999. Energy landscapes of receptor-ligand bonds explored with dynamic force spectroscopy. *Nature*. 397:50–53.
20. Evans, E., A. Leung, D. Hammer, and S. Simon. 2001. Chemically distinct transition states govern rapid dissociation of single l-selectin bonds under force. *Proc. Natl. Acad. Sci. USA*. 98:3784–3789.
21. Grubmueller, H., B. Heymann, and P. Tavan. 1996. Ligand binding: molecular mechanics calculation of the streptavidin-biotin rupture force. *Science*. 271:997–999.
22. Heymann, B., and H. Grubmueller. 1999. AN02/DNP-hapten unbinding forces studied by molecular dynamics atomic force microscopy simulations. *Chem. Phys. Lett*. 303:1–9.
23. Heymann, B., and H. Grubmueller. 2001. Molecular dynamics force probe simulations of antibody/antigen unbinding: entropic control and nonadditivity of unbinding forces. *Biophys. J*. 81:1295–1313.
24. Izrailev, S., S. Stepaniatis, M. Balsera, Y. Oono, and K. Schulten. 1997. Molecular dynamics study of unbinding of the avidin-biotin complex. *Biophys. J*. 72:1568–1581.
25. Paci, E., A. Caflisch, A. Plueckthun, and M. Karplus. 2001. Forces and energetics of hapten-antibody dissociation: a biased molecular dynamics study. *J. Mol. Biol*. 314:589–605.
26. Isralewitz, B., M. Gao, and K. Schulten. 2001. Steered molecular dynamics and mechanical functions of proteins. *Curr. Opin. Struct. Biol*. 11:224–230.
27. Lu, H., B. Isralewitz, A. Krammer, V. Vogel, and K. Schulten. 1998. Unfolding of titin immunoglobulin domains by steered molecular dynamics simulation. *Biophys. J*. 75:662–671.
28. Paci, E., and M. Karplus. 1999. Forced unfolding of fibronectin type 3 modules: an analysis by biased molecular dynamics simulations. *J. Mol. Biol*. 288:441–459.
29. Paci, E., and M. Karplus. 2000. Unfolding proteins by external forces and high temperatures: the importance of topology and energetics. *Proc. Natl. Acad. Sci. USA*. 97:6521–6526.
30. Best, R., S. Fowler, J. Toca-Herrera, A. Steward, E. Paci, and J. Clarke. 2003. Mechanical unfolding of a titin Ig domain: structure of transition state revealed by combining atomic force microscopy, protein engineering and molecular dynamics simulations. *J. Mol. Biol*. 330: 867–877.
31. Brockwell, D., E. Paci, R. Zinober, G. Beddard, P. Olmsted, D. Smith, R. Perham, and S. Radford. 2003. Pulling geometry defines the mechanical resistance of a $\beta$-sheet protein. *Nat. Struct. Biol*. 10:731–737.
32. Carrion-Vazquez, M., H. Li, H. Lu, P. Marszalek, A. Oberhauser, and J. Fernandez. 2003. The mechanical stability of ubiquitin is linkage-dependent. *Nat. Struct. Biol*. 10:738–743.
33. Curcio, R., A. Caflisch, and E. Paci. 2005. Change of the unbinding mechanism upon a mutation: a molecular dynamics study of an antibody-hapten complex. *Protein Sci*. 14:2499–2514.
34. Fowler, S., R. Best, J. Toca-Herrera, T. Rutherford, A. Steward, E. Paci, M. Karplus, and J. Clarke. 2002. Mechanical unfolding of a titin Ig domain: structure of unfolding intermediate revealed by combining AFM, molecular dynamics simulations, NMR and protein engineering. *J. Mol. Biol*. 322:841–849.
35. Krammer, A., H. Lu, B. Isralewitz, K. Schulten, and V. Vogel. 1999. Forced unfolding of the fibronectin type III module reveals a tensile

molecular recognition switch. *Proc. Natl. Acad. Sci. USA*. 96:1351–1356.

36. Marszalek, P., H. Lu, H. Li, M. Carrion-Vazquez, A. Oberhauser, K. Schulten, and J. Fernandez. 1999. Mechanical unfolding intermediates in titin modules. *Nature*. 402:100–103.
37. Sapra, K. T., H. Besir, D. Oesterhelt, and D. J. Mueller. 2006. Characterizing molecular interactions in different bacteriorhodopsin assemblies by single-molecule force spectroscopy. *J. Mol. Biol.* 355: 640–650.
38. Janovjak, H., D. J. Mueller, and A. L. Humpris. 2005. Molecular force modulation spectroscopy revealing the dynamic response of single bacteriorhodopsins. *Biophys. J.* 88:1423–1431.
39. Kessler, M., and H. E. Gaub. 2006. Unfolding barriers in bacteriorhodopsin probed from the cytoplasmic and the extracellular side by AFM. *Structure*. 14:521–527.
40. Kessler, M., K. E. Gottschalk, H. Janovjak, D. J. Mueller, and H. E. Gaub. 2006. Bacteriorhodopsin folds into the membrane against an external force. *J. Mol. Biol.* 357:644–654.
41. Lazaridis, T. 2003. Effective energy function for proteins in lipid membranes. *Proteins Struct. Funct. Genet*. 52:176–192.
42. Grigorieff, N., T. A. Ceska, K. H. Downing, J. M. Baldwin, and R. Henderson. 1996. Electron-crystallographic refinement of the structure of bacteriorhodopsin. *J. Mol. Biol.* 259:393–421.
43. Sali, A., and T. L. Blundell. 1993. Comparative protein modelling by satisfaction of spatial restraints. *J. Mol. Biol.* 234:779–815.
44. Brooks, B. R., R. E. Bruccoleri, B. D. Olafson, D. J. States, S. Swaminathan, and M. Karplus. 1983. CHARMM: a program for macromolecular energy, minimization, and dynamics calculations. *J. Comput. Chem.* 4:187–217.
45. Neria, E., S. Fischer, and M. Karplus. 1996. Simulation of activation free energies in molecular dynamics system. *J. Chem. Phys.* 105:1902–1921.
46. Lazaridis, T., and M. Karplus. 1999. Effective energy function for proteins in solution. *Proteins Struct. Funct. Genet*. 35:133–152.
47. Bell, G. I. 1978. Models for the specific adhesion of cells to cells. *Science*. 200:618–627.
48. Bayas, M. V., K. Schulten, and D. Leckband. 2003. Forced detachment of the CD2–CD58 complex. *Biophys. J.* 84:2223–2233.
49. Craig, D., M. Gao, K. Schulten, and V. Vogel. 2004. Tuning the mechanical stability of fibronectin type III modules through sequence variations. *Structure*. 12:21–30.
50. West, D., P. D. Olmsted, and E. Paci. 2006. Mechanical unfolding revisited through a simple but realistic model. *J. Chem. Phys.* 124: 154909.
51. Cisneros, D. A., D. Oesterhelt, and D. J. Mueller. 2005. Probing origins of molecular interactions stabilizing the membrane proteins halorhodopsin and bacteriorhodopsin. *Structure*. 13:235–242.
52. DeLano, W. 2002. The PyMOL molecular graphics system. http://www.pymol.org.